

10.1071/CH05246_AC

©CSIRO 2005

Accessory Publication: Aust. J. Chem., 2005, 58(11), 767–777.

ACCESSORY MATERIALS

Driving the Localized-to-Delocalized Transition in Unsymmetrical Dinuclear Ruthenium Mixed-Valence Complexes

Deanna M. D'Alessandro and F. Richard Keene

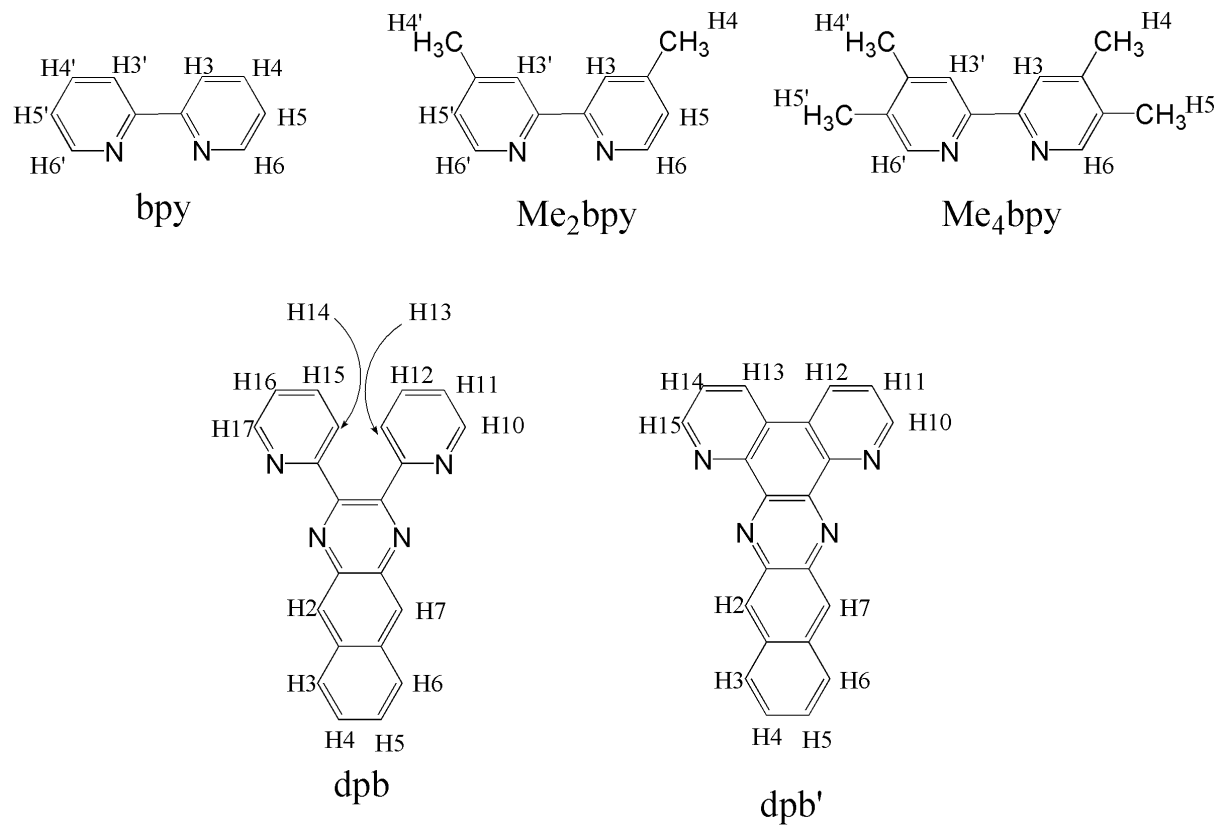


Figure S1. ^1H NMR numbering scheme for the terminal and bridging ligands.

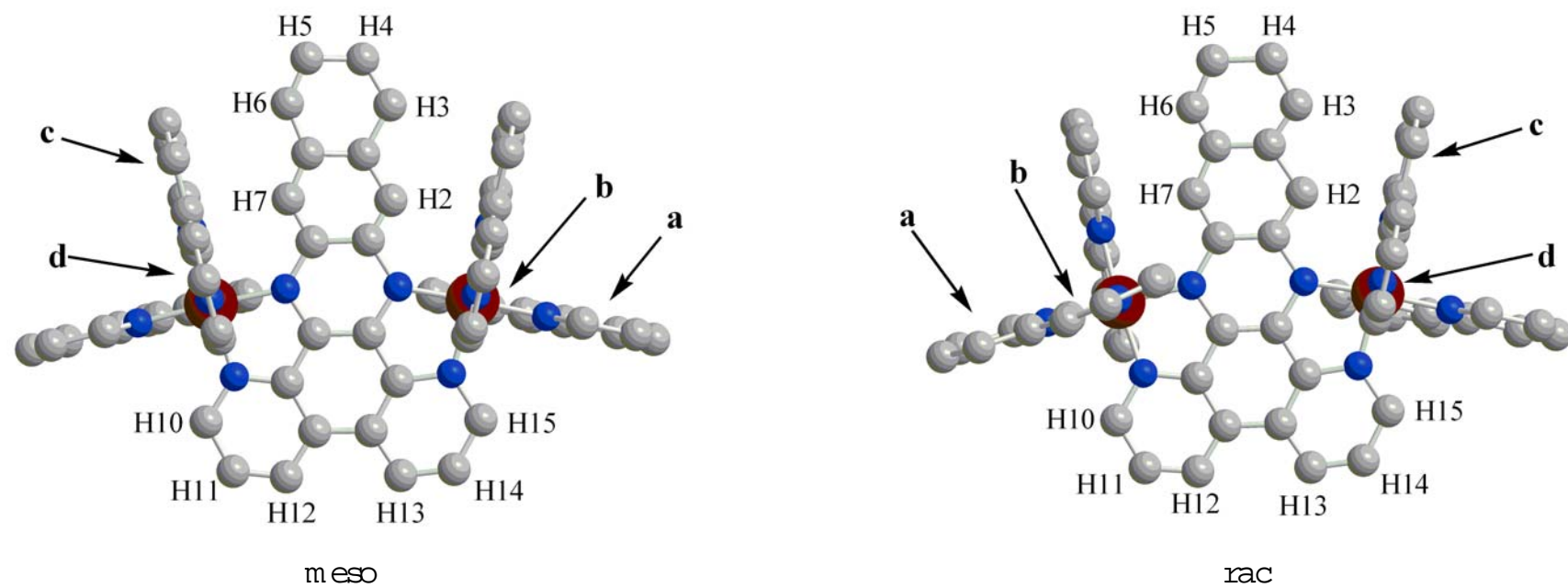


Figure S2. (a) Chem 3D representations of *meso*- $(\Lambda\Lambda)$ - and *rac*- $(\Delta\Delta)$ - $[\{Ru(bpy)_2\}_2(\mu-dpb')]^{4+}$. Hydrogen atoms are omitted for clarity.

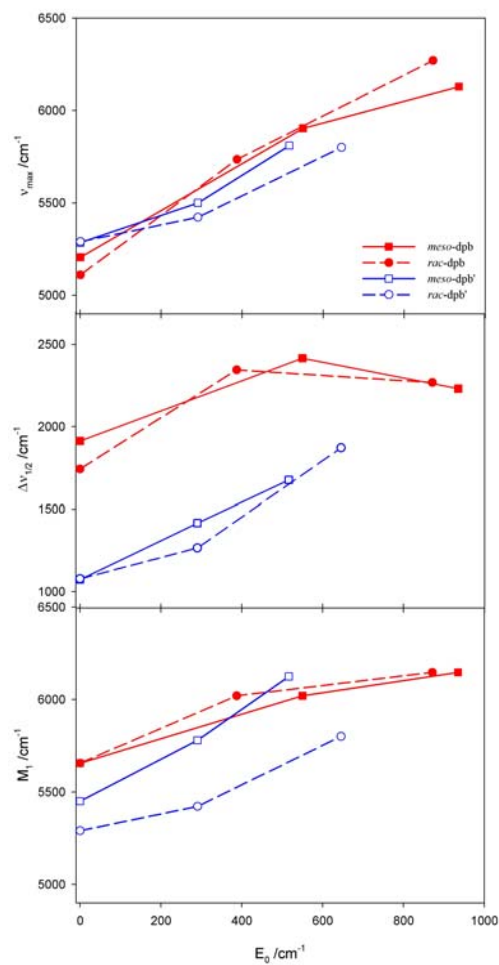


Figure S3. (a) v_{max} (b) $\Delta v_{1,2}$ and (c) M_1 as a function of E_0 for the series $[\{\text{Ru}(\text{ppy})_2\}(\mu\text{-BL})\{\text{Ru}(\text{pp})_2\}]^{5+}$ $\{\text{BL} = \text{dpb}, \text{dpb}'; \text{pp} = \text{bpy}, \text{Me}_2\text{bpy}, \text{Me}_4\text{bpy}\}$. Error bars are omitted for clarity.

Table S1. ^1H Chemical shifts (ppm) for the diastereoisomeric forms of $[\{\text{Ru}(\text{bpy})_2\}_2(\mu\text{-dpb})]^{4+}$ (CD_3CN , PF_6^- salts).

		<i>meso</i> ($\Delta\Delta/\Delta\Delta$)	<i>rac</i> ($\Delta\Delta/\Delta\Delta$)
bpy ring a ^A (over bpy)	H3'	8.27	8.57
	H4'	8.13	8.25
	H5'	7.70	7.62
	H6'	7.97	8.00
bpy ring b ^A (over ppz)	H3	8.72	8.57
	H4	8.19	8.05
	H5	7.25	7.01
	H6	7.72	7.54
bpy ring c ^A (over bpy)	H3'	8.69	8.63
	H4'	8.24	8.21
	H5'	7.48	7.54
	H6'	7.75	7.68
bpy ring d ^A (over BL)	H3	8.06	8.45
	H4	7.76	8.02
	H5	7.15	7.25
	H6	6.97	7.34
dpb ^B	H2/7	8.24	8.07
	H3/6	7.33	7.15
	H4/5	7.58	7.57
	H10/15	8.16	8.18
	H11/14	7.98	7.99
	H12/13	9.33	9.26

^A H6 (dd; $J = 5, 1.5$ Hz); H5 (dd; $J = 8, 5$ Hz); H4 (dd; $J = 8, 8$ Hz); H3 (dd; $J = 8, 1.5$ Hz).

^B H2/7 (s); H3/6 (dd, $J = 5, 1.5$ Hz); H4/5 (dd, $J = 10, 8$ Hz); H10/15 (d, $J = 8$ Hz); H11/14 (dd, $J = 8, 1.5$ Hz); H12/13 (d, $J = 8$ Hz).

¹H NMR spectral assignments for [Ru(bpy)₂(μ-dpb')]⁴⁺

The *meso* and *rac* diastereoisomers possess C_s and C_2 point group symmetries, respectively, and may be distinguished on the basis of differential anisotropic interactions experienced by the bpy protons depending upon the stereochemical relationship of the two metal centres. In addition, the dpb' ligand exhibits seven magnetically non-equivalent proton resonances. The point group symmetries of both diastereoisomers require two non-equivalent bpy ligands, with the two halves of each being magnetically non-equivalent and hence four different environments for the py ligands (denoted *ring a-d* in Figure S2), two over the bridge (*rings b* and *d*) and two directed away from the bridge (*rings a* and *c*).

The H5 and H6 protons (*rings b* and *d* oriented over the bridge) experience the most pronounced shifts between the two diastereoisomeric forms. In the *rac* diastereoisomer, bpy *ring b* is oriented over the plane of the dpb ligand and the bpy ligand across the bridge such that the H5 and H6 protons of bpy *ring b* experience increased diamagnetic anisotropic effects. The H5 proton of *ring b* was assigned as the most upfield resonance at 7.01 ppm ($J = 8, 5$ Hz, dd) while H6 (*ring b*) was assigned as the 7.54 ppm ($J = 5, 1.5$ Hz, dd) resonance. By comparison, the H5 and H6 protons of bpy *ring b* are oriented approximately in the plane and thus in the deshielding cone of the equivalent bpy across the bridge in the *meso* diastereoisomer. The H5' proton of *ring d*, which is situated over the plane of the dpb' ligand and approximately parallel to the magnetically equivalent bpy across the bridge, experiences the relatively greatest anisotropic effect and is assigned as the most upfield resonance at 7.25 ppm ($J = 8, 5$ Hz, dd).

The assignment of the remaining resonances was achieved by ¹H COSY experiments and the differential anisotropic effects.

Table S2. Reduction potentials (in mV relative to the Fc^+/Fc^0 couple) for $[\{\text{Ru}(\text{bpy})_2\}(\mu\text{-dpb})\{\text{Ru}(\text{pp})_2\}]^{4+}$ in 0.1 M $[(n\text{-C}_4\text{H}_9)_4\text{N}]\text{PF}_6/\text{CH}_3\text{CN}$.

pp	Diastereoisomer	E_{red1}	E_{red2}	E_{red3}	E_{red4}	E_{red5}	E_{red6}
Me ₄ bpy	<i>meso</i>	-664	-1252	-1604 -1768 -1893 -2004	-2096	-2201	-2412
	<i>rac</i>	-656	-1304	-1892	-2125	-2202	-2404
Me ₂ bpy	<i>meso</i>	-644	-1292	-1880	-1996	-2156	-2316
	<i>rac</i>	-644	-1288	-1896	-1996	-2164	-2300
bpy	<i>meso</i>	-624	-1268	-1888	-2116	-2240	-2552
	<i>rac</i>	-624	-1260	-1876		-2252	-2640

Table S3. Reduction potentials (in mV relative to the Fc^+/Fc^0 couple) for $[\{\text{Ru}(\text{bpy})_2\}(\mu\text{-dpb}')\{\text{Ru}(\text{pp})_2\}]^{4+}$ in 0.1 M $[(n\text{-C}_4\text{H}_9)_4\text{N}]\text{PF}_6/\text{CH}_3\text{CN}$.

pp	Diastereoisomer	E_{red1}	E_{red2}	E_{red3}	E_{red4}	E_{red5}	E_{red6}
Me ₄ bpy	<i>meso</i>	-496	-1148	-1880	-2172	-2448	-2663
	<i>rac</i>	-496	-1148	-1876	-2160	-2432	-2743
Me ₂ bpy	<i>meso</i>	-484	-1132	-1883	-1976	-2157	-2260
	<i>rac</i>	-496	-1128	-1868	-1981	-2144	-2272
bpy	<i>meso</i>	-464	-1116	-1888	-2180	-2716	
	<i>rac</i>	-452	-1096	-1884	-2192	-2720	

Table S5. NIR spectral data of the reduced absorption spectra (ϵ/ν vs. ν) for $[\{\text{Ru}(\text{bpy})_2\}(\mu\text{-BL})\{\text{Ru}(\text{pp})_2\}]^{5+}$ {BL = dpb, dpb'} at -35°C , respectively. The parameters for the overall NIR band envelopes are shown in bold type, and details of the deconvoluted bands are in normal type.

pp	Diastereoisomer	BL = dpb					BL = dpb'				
		ν_{\max} ± 10 /cm ⁻¹	$(\epsilon/\nu)_{\max}$ ± 0.001 /M ⁻¹	$\Delta\nu_{1/2}$ ± 10 /cm ⁻¹	M_0 /M ⁻¹	M_1 /cm ⁻¹	ν_{\max} ± 10 /cm ⁻¹	$(\epsilon/\nu)_{\max}$ ± 0.001 /M ⁻¹	$\Delta\nu_{1/2}$ ± 10 /cm ⁻¹	M_0 /M ⁻¹	M_1 /cm ⁻¹
Me ₄ bpy	<i>meso</i>	6125	0.141	2230	331	6150	5810	0.223	1675	484	8640
		3925	0.005	255	0.372		2513	0.050	2399	9.36	
		4648	0.006	1574	9.47		5849	0.211	1501	337	
		6140	0.137	2193	317		5300	0.020	565	12.2	
		7905	0.004	1035	4.4		7054	0.030	1429	46.1	
							9298	0.029	793	11.4	
	<i>rac</i>	6130	0.144	2270	350	6125	5800	0.165	1870	357	5930
		2398	0.026	2916	7.95		2513	0.049	2399	9.15	
		6112	0.142	2274	338		5849	0.206	1501	329	
		8061	0.003	944	3.29		5300	0.019	565	11.9	
						7054	0.029	1429	45.0		
						9298	0.029	793	11.2		
Me ₂ bpy	<i>meso</i>	5905	0.179	2415	386	6020	5500	0.518	1415	512.1	5725
		3897	0.013	649	3.40		4018	0.030	659	11.0	
		5896	0.148	2182	338		5488	0.489	1099	571	
		5022	0.013	849.6	12.1		6261	0.086	756	69.4	
		7464	0.017	1733	32.2		6754	0.066	1180	83.6	
							9289	0.072	976	35.4	
	<i>rac</i>	5540	0.230	2345	559	5780	5420	0.332	1265	735	7570
		3902	0.013	447	2.38		4062	0.006	330	1.42	
		4916	0.012	629	8.62		5086	0.008	382	3.30	
		5556	0.222	2186	494		5444	0.314	1074	358	
7117		0.027	1944	56.4		6180	0.083	795	70.2		
						6648	0.058	1253	78.3		
						9212	0.034	961	19.0		

Table S6. Spectroelectrochemical data for $[\{\text{Ru}(\text{bpy})_2\}_2(\mu\text{-BL})]^{4+}$ {BL = dpb or dpb'} in 0.1 M $[(n\text{-C}_4\text{H}_9)_4\text{N}]\text{PF}_6/\text{CH}_3\text{CN}$. The parameters of the IVCT transitions are indicated in bold type.^A

BL		dpb		dpb'	
Diastereoisomer	<i>n</i> +	$\nu_{\text{max}}/\text{cm}^{-1}$	$(\epsilon/\nu)_{\text{max}}/\text{M}^{-1}$	$\nu_{\text{max}}/\text{cm}^{-1}$	$(\epsilon/\nu)_{\text{max}}/\text{M}^{-1}$
<i>meso</i>	4	<i>sh</i> 13070	0.295	<i>sh</i> 11670	0.264
		15530	1.444	13880	2.041
		23520	1.081	16900	0.213
		24460	0.982	24780	1.352
		26870	1.569	29140	1.509
		29450	1.435		
	5	5205	0.306	5285	0.808
		15120	0.767	9253	0.099
		<i>sh</i> 17370	0.450	11420	0.359
		25920	1.474	13930	0.959
				21660	0.378
				22770	0.473
6	~15000		14210	0.149	
	16870	0.225	20850	0.834	
	25230	1.270	22140	0.775	
			27440	1.533	
<i>rac</i>	4	<i>sh</i> 13070	0.226	<i>sh</i> 11770	0.253
		15420	1.415	13870	1.896
		20480	0.349	16850	0.166
		23470	1.110	24780	1.215
		<i>sh</i> 24400	0.987	29150	1.324
		26820	1.491		
	5	4998	0.457	5290	0.722
		14980	0.683	9223	0.087
		25700	1.636	11250	0.279
				13920	0.905
				21630	0.349
				22680	0.436
6	17760	0.127	12730	0.318	
	25170	1.948	15880	0.200	
			20850	0.646	
			22180	0.619	
			27430	1.306	

^A Errors in ν_{max} and $(\epsilon/\nu)_{\text{max}}$ are $\pm 10 \text{ cm}^{-1}$ and $\pm 0.001 \text{ M}^{-1}$, respectively.